DMD Fast Forward. Published on June 11, 2018 as DOI: 10.1124/dmd.118.080770
This article has not been copyedited and formatted. The final version may differ from this version.

Drug Metabolism and Disposition: Article

Transport Kinetics, Selective Inhibition, and Successful Prediction of *In Vivo* Inhibition of Rat Hepatic Oatps

Kazuya Ishida, Mohammed Ullah, Beáta Tóth, Viktoria Juhasz, and Jashvant D. Unadkat

Department of Pharmaceutics, University of Washington, Seattle, Washington, U.S.A (K.I., J.D.U)

Cellular Transport Group, Pharmaceutical Sciences, Roche Innovation Centre Basel, F. Hoffmann-La Roche Ltd, Basel, Switzerland (M.U.)

SOLVO Biotechnology, Budaörs, Hungary (B.T., V.J.)

a) Running Title: Identification of selective inhibitors of rat hepatic Oatps

b) Address for correspondence: Jashvant D. Unadkat

Department of Pharmaceutics

Box 357610, University of Washington

Seattle, WA 98195

Telephone: (206) 543-9434, Fax: (206) 543-3204

E-mail: jash@u.washington.edu

c) Number of

Text Pages:	28
Tables:	3
Figures:	5
Supplemental Tables:	0
Supplemental Figures	2
References:	16
Words in Abstract:	249/250
Words in Introduction:	269/750
Words in Discussion:	1184/1500

d) Nonstandard Abbreviations: BSP; sulfobromophthalein, CL_{int}; intrinsic clearance, DDI; drug-drug interactions, IC_{50}; the half maximal inhibitory concentration, K_m; Michaelis-Menten constant, OATP/Oatp; organic anion transporting polypeptide, OLM; olmesartan acid, Rif SV; rifamycin SV, RSV; rosuvastatin, SCRH; sandwich-cultured rat hepatocytes, TCA; taurocholic

acid, V_{max}; maximum velocity of the uptake

DMD Fast Forward. Published on June 11, 2018 as DOI: 10.1124/dmd.118.080770
This article has not been copyedited and formatted. The final version may differ from this version.

Abstract

For successful *in vitro*-to-*in vivo* extrapolation (IVIVE) of hepatic drug uptake and DDI, it is important to characterize the kinetic properties of the individual transporters involved, their fraction (ft) contribution to hepatic uptake, and their selective inhibitors. Here, we characterized the *in vitro* transport kinetics of two model drugs, rosuvastatin (RSV) and olmesartan acid (OLM), by rat hepatic organic anion transporting polypeptides (Oatp1a1, 1a4 and 1b2) and identified selective inhibitors of these transporters. [^{3}H]-RSV was transported by Oatp1a1, 1a4 and 1b2, and their K_m values were estimated to be 9.61, 67.2, and 28.1 μM, respectively. In contrast, [^{3}H]-OLM was transported by only Oatp1b2 (K_m: 72.8 μM). Digoxin (IC_{50}: 0.107 μM) and rifamycin SV (IC_{50}: 0.140 and 0.088 μM for RSV and OLM, respectively) were potent and selective inhibitors of Oatp1a4 and 1b2, respectively, whilst glyburide (100 μM) completely inhibited all three rat hepatic Oatps. These inhibitors can therefore be used alone and in combination to determine the contribution of each Oatp to hepatic influx. In addition, the magnitude of *in vivo* inhibition of sinusoidal uptake clearance of RSV by rifampin was well predicted using rifampin IC_{50} profiles for each Oatps and RSV ft by each Oatp. This is the first report to: 1) detail the transport kinetics of RSV and OLM by rat hepatic Oatps; 2) identify selective inhibitor concentrations of rat Oatps; 3) demonstrate successful prediction of the magnitude of transporter-mediated *in vivo* DDI from IC_{50} profiles of an inhibitor and ft of a drug by each transporter.

DMD Fast Forward. Published on June 11, 2018 as DOI: 10.1124/dmd.118.080770
This article has not been copyedited and formatted. The final version may differ from this version.

Introduction

The rat is commonly used as a preclinical species in drug development, pharmacokinetics and toxicity studies. In addition, the rat is often used when conducting proof-of-concept or mechanistic pharmacokinetic studies. For example, we have recently shown that the *in vivo* hepatobiliary clearances and hepatic concentrations of rosuvastatin (RSV) in rats can be predicted using transporter-expressing cells and sandwich-cultured rat hepatocytes (SCRH) (Ishida et al., 2018). However, in order to correctly interpret and extrapolate hepatic clearance obtained from *in vitro* systems to *in vivo*, it is important to have detailed characterization of transport kinetics (e.g., the Michaelis-Menten constant (K_m)) of rat hepatic Oatps (Oatp1a1, 1a4 and 1b2) and their relative contribution to hepatic drug uptake using methods employing selective inhibition or *in vitro*-to-*in vivo* scaling of transporter-mediated clearance using quantitative proteomics. Although well-established when determining CYP-P450 mediated fraction metabolized, due to lack of selective inhibitors of transporters, this approach ihas had limited success in determining fraction transported by hepatic transporters. To this end, we characterized rat hepatic Oatp transport kinetics of two model drugs (RSV and olmesartan acid (OLM)) and identified selective inhibitors of rat Oatps that can be used to quantify the contribution of each rat hepatic Oatp towards overall Oatp-mediated hepatic uptake. In addition,, we assessed whether the *in vivo* inhibition of RSV hepatic uptake clearance by rifampin (a known inhibitor of rat Oatps), determined in our positron emission tomography (PET) imaging study (He et al., 2014), could be predicted from *in vitro* Oatp inhibition profiles (the half maximal inhibitory concentrations (IC_{50}) profiles) of rifampin and the ft of RSV by the various Oatps estimated using quantitative proteomics.

DMD Fast Forward. Published on June 11, 2018 as DOI: 10.1124/dmd.118.080770
This article has not been copyedited and formatted. The final version may differ from this version.

Marerials and Methods

Materials. RSV was purchased from Cayman Chemicals (Ann Arbor, MI). OLM was kindly provided from Daiichi-Sankyo Co. Ltd (Tokyo, Japan). [^{3}H]-RSV sodium salt (20 mCi/mmol, radiochemical purity 99%), [^{3}H]-OLM (10 mCi/mmol, radiochemical purity 99%, [^{3}H]-estradiol 17β-D-glucuronide (E17βG) (50 mCi/mmol, radiochemical purity 99%), and [^{3}H]-taurocholic acid (TCA) (10 mCi/mmol, radiochemical purity 99%) were purchased from American Radiolabeled Chemicals (St. Louis, MO). Rifampin, rifamycin SV sodium salt, ibuprofen, indomethacin, sulfobromophthalein (BSP) disodium salt, quinidine hydrochloride monohydrate, quinine hydrochloride dihydrate, glycyrrhizic acid, enalapril, and fexofenadine hydrochloride were purchased from Sigma Aldrich (St. Louis, MO). Celiprolol hydrochloride and cyclosporin A were purchased from Toronto Research Chemicals (Toronto, Ontario, Canada). Digoxin was purchased from Tokyo Kasei America. Glyburide was purchased from Calbiochem (La Jolla, CA). All other chemicals were of reagent or analytical grade and purchased from other commercial suppliers.

RSV and OLM Uptake into Ntcp- and Oatp-expressing Cells. CHO-Ntcp, CHO-Oatp1a1, HEK293-Oatp1a4, HEK293-Oatp1b2, and their corresponding mock-transfected cells were a gift from SOLVO Biotechnology (Budaörs, Hungary). CHO-Ntcp, CHO-Oatp1a1, and CHO-mock cells, grown in 75 cm^2 flasks, were harvested using trypsin, and were plated at a density of 0.5 × 10^6 cells/well in 24-well plates. These cells were incubated with 5 mM of sodium butyrate about 24 hr before conducting the transport experiments. HEK293-Oatp1a4, HEK293-Oatp1b2, and HEK293-mock cells, grown in 75 cm^2 flask with 3 μg/mL puromycin, were harvested using trypsin, and plated at a density of 0.5 × 10^6 cells/well in 24-well poly-D-lysine coated plates. These cells were also incubated with 3 μg/mL puromycin 24 hr before conducting the transport experiments. The cells were washed three times with pre-warmed Krebs-Henseleit (KH) buffer,

DMD Fast Forward. Published on June 11, 2018 as DOI: 10.1124/dmd.118.080770
This article has not been copyedited and formatted. The final version may differ from this version.

then pre-incubated (at 37 °C for 10 min) with the KH buffer in the absence or presence of the chosen inhibitor (see below). After pre-incubation, the cells were incubated (at 37 °C for 5-120 sec) with 500 µL of 0.01-1000 µM RSV (containing 0.2 µCi/well [^{3}H]-RSV) or OLM (containing 0.2 µCi/well [^{3}H]-OLM) with or without the chosen inhibitor. The KH buffer containing the drug was aspirated, and the cells were washed three times with ice-cold KH buffer, and then 1 mL of 2% SDS were added to lyse the cells. The total radioactivity in the samples was measured using a liquid scintillation counter (Perkin Elmer, Waltham, MA). The total protein concentration of cell lysate was measured with Pierce™ BCA Protein Assay Kit (Pierce Biotechnology, Rockford, IL), according to the manufacturer's instructions. As a positive control, the uptake of TCA (for Ntcp, 0.5 µM TCA containing 0.2 µCi/well [^{3}H]-TCA) in the presence and absence of the extracellular Na^+ or the uptake of E17βG (for Oatps, 0.5 µM E17βG containing 0.2 µCi/well [^{3}H]-E17βG) in the absence and presence of 100 µM rifamycin SV were also determined.

Estimation of K_m and V_{max} of RSV and OLM. The K_m, the maximum velocity (V_{max}), and the diffusion rate constant (K_d) were estimated using the nonlinear regression package, Phoenix® (Certara, Princeton, NJ). The following equations were simultaneously fitted to the data (Chenu and Berteloot, 1993; Endres et al., 2009; Malo and Berteloot, 1991):

$$v_{Oatp} = \frac{V_{max} \cdot T \cdot (S_{cold}+T)^{H-1}}{K_m^H + (S_{cold}+T)^H} + K_d \cdot T \quad (1)$$

$$v_{mock} = K_d \cdot T \quad (2)$$

where v_{Oatp} and v_{mock} are the uptake rate of the drug into Oatp-expressing cells and mock-transfected cells, respectively. S_{cold} and T are the concentration of unlabeled and labeled drug, respectively. H is the Hill coefficient.

DMD Fast Forward. Published on June 11, 2018 as DOI: 10.1124/dmd.118.080770
This article has not been copyedited and formatted. The final version may differ from this version.

Estimation of IC_{50} of Inhibitors. The IC_{50} of several drugs towards RSV or OLM uptake was estimated using the nonlinear regression package, Phoenix® (Certara, Princeton, NJ). The following equations were simultaneously fitted to the data:

$$Uptake_{Oatp}(\%\ of\ max) = min + \frac{max-min}{1+([I]/IC_{50})^{H}} \quad (3)$$

$$Uptake_{mock}(\%\ of\ max) = min \quad (4)$$

where *max* and *min* are the maximum (fixed at 100%, i.e., uptake in the absence of the inhibitor) and minimum uptake (uptake in mock cells or when the inhibitor concentration greatly exceeds IC_{50} - expressed as % of max) of the drug, respectively. [*I*] and *H* are the inhibitor concentration and Hill coefficient, respectively.

Prediction of the Inhibitory Effect of Rifampin on *In Vivo* Sinusoidal Uptake Clearance of RSV in the Rat Liver. The *in vivo* sinusoidal uptake clearance of RSV in the presence of rifampin ($CL_{s,uptake}^{Rif(+)}$), at steady-state plasma rifampin concentration observed in our PET imaging study (9.4 μM), was estimated as follows:

$$CL_{s,uptake}^{Rif(+)} = \sum\left(CL_{uptake,i}^{Rif(-)} \cdot \%\ remaining\ activity\right) + CL_{passive}^{HEK293} \quad (5)$$

where $CL_{uptake,i}^{Rif(-)}$ is the *in vivo* predicted sinusoidal uptake clearance of RSV in the rat liver by each Oatp. That is, the predicted *in vivo* uptake clearance was obtained by the summation of the intrinsic *in vitro* uptake clearance of RSV (by Oatp1a1, 1a4, and 1b2) scaled up to that *in vivo* using the abundance of each Oatp in the Oatp-expressing cell line and *in vivo* (in the rat liver)

DMD Fast Forward. Published on June 11, 2018 as DOI: 10.1124/dmd.118.080770
This article has not been copyedited and formatted. The final version may differ from this version.

(data obtained from Ishida et al., and Wang et al., (Ishida et al., 2018; Wang et al., 2015)). $CL_{passive}^{HEK}$ is the passive diffusion clearance of RSV estimated from HEK293-mock cells (the mean K_d value in the present study). The *% remaining activity* of each Oatp in the presence of 9.4 μM rifampin was calculated from the IC_{50} profiles (see Figure 4) and the following equation:

$$\%\ remaining\ activity = \frac{Uptake_{Oatp}^{Rif(+)} - Uptake_{mock}}{Uptake_{Oatp}^{Rif(-)} - Uptake_{mock}} \quad (6)$$

where $Uptake_{Oatp}^{Rif(-)}$ is the RSV uptake into the Oatp-expressing cells in the absence of rifampin, and was fixed as 100%. $Uptake_{mock}$ is the RSV uptake (% of max) into the mock-transfected cells, and $Uptake_{Oatp}^{Rif(+)}$ is the RSV uptake (% of max) into the Oatp-expressing cells in the presence of 9.4 μM rifampin.

Statistical Analysis. The experimental data are shown as the mean ± standard deviation (SD). The parameters estimated from Phoenix are shown as the mean ± standard error (SE). Statistically significant differences between the various groups were determined by the Welch's t-test (corrected for multiple comparisons).

DMD Fast Forward. Published on June 11, 2018 as DOI: 10.1124/dmd.118.080770
This article has not been copyedited and formatted. The final version may differ from this version.

Results

Time-dependent Uptake of RSV or OLM into Ntcp- or Oatp-expressing Cells. We first evaluated TCA or E17βG uptake into Oatp- or Ntcp-expressing cells, and confirmed that these cell lines are functional (Supplemental Figure 1). Consistent with previous reports (Ho et al., 2006; Ishida et al., 2018), RSV was transported by Oatp1a1, 1a4, and 1b2, but not by Ntcp (Figure 1). RSV uptake by Oatp1a1 approached a plateau by 15 sec, whereas that by Oatp1a4 and 1b2 was linear for at least 15 sec. In contrast, OLM was transported by only Oatp1b2 and this uptake was linear up to at least 30 sec (Figure 1). Therefore, in subsequent experiments, we evaluated the 5-sec (Oatp1a1) and 15-sec (Oatp1a4 and 1b2) uptake of RSV or OLM (Oatp1b2 only).

Estimation of Kinetics of Uptake of RSV or OLM by CHO-Oatp1a1, HEK293-Oatp1a4, HEK293-Oatp1b2 Cells. As expected, the uptake of [^{3}H]-RSV and [^{3}H]-OLM was decreased with increasing unlabeled RSV and OLM concentration (representative experiments are shown in Figure 2). Oatp1a1 transported RSV with higher affinity than Oapt1a4 (Table 1). In addition, Oatp1b2 transported RSV with higher affinity than OLM (Table 1). The K_m values obtained informed the RSV and OLM concentrations used in the inhibition experiments described below. Also, the RSV K_m and V_{max} values were used to predict the *in vivo* inhibition of the sinusoidal uptake clearance of the drug by rifampin (see below).

Identification of Selective Inhibitors of RSV, E17βG, or OLM Uptake into Oatp-expressing Cells. In an initial screen conducted at a low (10 μM) and high (100 μM) inhibitor concentrations, ibuprofen (100 μM) and OLM (100 μM) appeared to be a selective inhibitor of Oatp1b2-mediated RSV uptake (Figure 3A). On the other hand, digoxin (10 μM) and quinine (10 μM) appeared to be a selective inhibitor of Oatp1a4-mediated RSV uptake. Rifampin (10 μM) inhibited Oatp1a4 and 1b2 only, whereas rifamycin SV (10 μM) inhibited only Oatp1a1- and

1b2-mediated RSV uptake. Glyburide inhibited all three rat hepatic Oatps (Figure 3A). BSP also inhibited all three rat hepatic Oatps, but 100 μM BSP did not completely inhibit all rat hepatic Oatps (Figure 3A). A similar trend was observed of inhibition of Oatp1a1- and 1a4-mediated E17βG uptake (Figure 3B) or of Oatp1b2-mediated OLM uptake (Figure 3C), except E17βG, but not RSV, uptake by Oatp1a1 was inhibited by 10 μM quinine (Figure 3A and B).

Determination of IC_{50} of Inhibitors of Rat Hepatic Oatps. Based on the above data and to confirm that the above inhibitors were selective inhibitors of the indicated Oatp, we determined their IC_{50} values using RSV and OLM as substrates. (Figure 4 and Supplemental Figure 2). While 100 μM rifampin completely inhibited Oatp1a4 and 1b2, at this concentration it also significantly inhibited Oatp1a1 (~by about 50%) (Figure 4A-D). Rifamycin SV (1 μM) completely inhibited Oatp1b2 but did not inhibit Oatp1a1 or 1a4 (Figure 4E-H). Digoxin (100 μM) completely inhibited Oatp1a4 but not Oatp1a1 or 1b2 (Figure 4I-L). Ibuprofen (1000 μM) did not inhibit Oatp1a4, but inhibited Oatp1a1 and Oatp1b2 (Supplemental Figure 2A-D). Quinine inhibited all Oatps when the concentration of the drug was greater than 20 μM (Supplemental Figure 2E-H). Although OLM is a selective substrate of Oatp1b2 (Figure 1), at 1000 μM it completely inhibited Oatp1b2 and partially inhibited Oatp1a1 but not Oatp1a4 (Supplemental Figure 2I-K). BSP inhibited Oatp1a4 less potently than Oatp1a1 or1b2, but inhibited all Oatps at >300 μM (Supplemental Figure 2L-O).

Prediction and verification of the Magnitude of Inhibition of *In Vivo* Sinusoidal Uptake Clearance of RSV in the Presence of 9.4 μM Rifampin. We predicted the *in vivo* inhibition of the sinusoidal uptake clearance of RSV in rats using the intrinsic clearance (V_{max}/K_m) and K_d (Table 2) and the abundance of Oatp protein in the rat liver and transfected cells (Ishida et al., 2018; Wang et al., 2015). Then, we compared the predicted inhibition to our previous *in vivo* PET imaging study (He et al., 2014). The magnitude of inhibition of sinusoidal uptake clearance of

RSV by rifampin was well predicted (Table 3).

DMD Fast Forward. Published on June 11, 2018 as DOI: 10.1124/dmd.118.080770
This article has not been copyedited and formatted. The final version may differ from this version.

Discussion

Three Oatps, Oatp1a1, 1a4, and 1b2, are expressed in the rat liver, and their protein expression, as determined by quantitative targeted proteomics, are similar (Wang et al., 2015). Therefore, any pharmacokinetic studies or hepatic efficacy/toxicity of Oatp substrate drugs in the rat must include consideration of these transporters. Here, we estimated for the first time the transport kinetic parameters of RSV and OLM by three rat hepatic Oatps. Since, several OATPs/Oatps have been shown to have multiple binding sites (Shirasaka et al., 2014; Westholm et al., 2009), we first determined if this was the case for the uptake of RSV or OLM by the three rat Oatps. To enhance our ability to discern multiple binding sites, our experimental design was deliberately rich in data points (18-21 concentrations, in duplicate, densly scattered over a wide concentration range). Although we incorporated a second binding site (i.e. K_m and V_{max}) into our model, the 95% confidence interval of these additional parameters contained zero and therefore were deemed not to be reliable (data not shown). Hence, our final kinetic model included one binding site for transport (to estimate the K_m, V_{max} and Hill coefficient) as well as passive diffusion (to estimate the K_d) (Eq. 1 and 2).

To determine the contribution of each OATP/Oatp in the uptake of drugs into hepatocytes or *in vivo*, it is important to conduct inhibition studies with selective transporters of each Oatp. However, to date, such selective inhibitors have not been available as most drugs appear to be non-selective inhibitors of all Oatps. Here we found that rifamycin SV (1 μM) and digoxin (20 μM) were selective and potent inhibitors of Oatp1b2 (IC_{50} 0.14 μM) and Oatp1a4 (IC_{50} 0.1 μM), respectively (Figure 4), For the remaining inhibitors, although they were found to be potent inhibitors of some Oatps (e.g. 10 μM quinine), when they were tested at concentrations that completely inhibited those transporters, they partially inhibited other Oatps (Figure 3). Thus, they were not considered selective. BSP (>300 μM) and glyburide (100 μM) non-selectively inhibited

all the Oatps and were considered pan-Oatp inhibitors. While the IC_{50} value of an inhibitor is important, the ability of that inhibitor to inhibit the *in vivo* clearance of a victim drug mediated by an Oatp(s) depends on the plasma concentration of the inhibitor achieved relative to its IC_{50}. Thus, although some of the inhibitors studied, at first sight, may not appear to be potent inhibitors of Oatps, if the unbound portal vein plasma concentrations of the inhibitor (at the doses used) exceeds its IC_{50} value for an Oatp, then the inhibitor will inhibit that hepatic Oatp *in vivo*. In addition, with the inhibitors tested, substrate-dependent inhibition of RSV, OLM, and E17βG was not observed (Figure 3 and 4, Table 2, and Supplemental Figure 2).

Previous Oatp inhibition studies have focused on only one or two rat hepatic Oatps (Fattinger et al., 2000; Ismair, 2003; Shitara et al., 2002). Our findings are generally consistent with these previous reports (Fattinger et al., 2000; Shitara et al., 2002) but expand on these reports by including studies on Oatp1b2. However, we did observe some differences between the present study and a previous report by Shitara et al. (Shitara et al., 2002). Shitara et al. evaluated the inhibitory effect of many compounds on Oatp1a1- and Oatp1a4-mediated uptake of E17βG and digoxin, respectively (Shitara et al., 2002). Consistent with our data, Oatp1a1- and 1a4 were not inhibited by 10 μM indomethacin, but they found that Oatp1a1, but not Oatp1a4, was inhibited when the indomethacin concentration was increased to 100 μM. In the present study, we found that 100 μM indomethacin inhibited all three rat hepatic Oatps (Figure 3). Unlike us, they found that quinidine (100 μM) inhibited Oatp1a1 but not Oatp1a4 activity, but their IC_{50} profiles of inhibition by quinidine showed that IC_{50} values of quinidine for Oatp1a1 and 1a4 are similar. (Shitara et al., 2002). We found that quinidine (100 μM) slightly inhibited both Oatp1a1 and 1a4 activity but not Oatp1b2 activity (Figure 3). In all cases, we observed inhibitory effect of these drugs at lower concentrations than previously reported. One reason for this difference may be that we pre-incubated the cells with the inhibitors while the previous investigators did not.

DMD Fast Forward. Published on June 11, 2018 as DOI: 10.1124/dmd.118.080770
This article has not been copyedited and formatted. The final version may differ from this version.

In the present study, we were successful in identifying selective inhibitors of Oatp1b2 and 1a4, but not Oatp1a1. Therefore, we propose the following experimental design to distinguish Ntcp-, Oatp-, and passive diffusion-mediated uptake of the drug into rat hepatocytes (*in vitro* and potentially *in vivo*) (Figure 5). As usual, the contribution of Ntcp-dependent uptake can be estimated by the difference in the drug uptake in the presence and absence of extracellular Na^+. Since 1 μM rifamycin SV and 20 μM digoxin selectively and completely inhibited Oatp1b2 and Oatp1a4, respectively (Figure 4), the contribution of Oatp1b2 and 1a4 can be estimated by using the selective inhibitor 1 μM rifamycin SV and 20 μM digoxin, respectively, under the extracellular Na^+-free condition (Figure 4 and 5; Table 2). Glyburide (or BSP) is a pan inhibitor of rat hepatic Oatps (Figure 3); therefore, the passive diffusion-mediated uptake of the drug can be estimated in the presence of 100 μM glyburide (or 300 μM BSP) under the Na^+-free condition. Although, we did not identify a selective inhibitor of Oatp1a1, its contribution can be obtained by taking the difference in drug uptake in the presence of digoxin (20 μM) plus rifamycin SV (1 μM) and glyburide (100 μM). This strategy assumes that these inhibitors will not inhibit other transporters/metabolizing enzymes that my also transport/metabolize the drug of interest.

To predict the magnitude of the transporter-mediated drug-drug interactions (DDI), the fraction of a drug transported (ft) by a particular transporter needs to be estimated (Hsiao and Unadkat, 2014; Li et al., 2014; Prasad and Unadkat, 2015). In our previously published rat [^{11}C]-RSV PET imaging study, the *in vivo* sinusoidal uptake clearance of RSV was decreased ~50% by rifampin (plasma concentration 9.4 μM) (Table 3) (He et al., 2014). The magnitude of this *in vivo* RSV-rifampin DDI was well predicted (Table 3) by our *in vitro* studies using the Oatp IC_{50} profiles of rifampin and the *in vivo* RSV ft predicted using the *in vitro* intrinsic clearance (V_{max}/K_m) by each Oatp (Table 1) and the abundance of the respective Oatp protein in the rat liver and Oatp-expressing cells previously reported (Ishida et al., 2018; Wang et al., 2015). This

approach can be used to predict transporter-based DDI at any tissue:blood barrier where transporters are important in the distribution or elimination of a drug (Hsiao and Unadkat, 2012; 2014).

In conclusion, this is the first report to estimate the transport kinetic parameters of RSV and OLM by rat hepatic Oatps and identify selective inhibitors of rat Oatp1b2 and Oatp1a4. We also provide a strategy to determine the contribution of Oatp1a1, 1a4, and 1b2 in the hepatic uptake of drugs. In addition, we show for the first time the magnitude of *in vivo* DDI with Oatp substrates can be predicted from in vivo studies by determining the ft of the victim drugs., quantitative proteomics, and inhibitory (IC_{50}) profile(s) of the inhibitor.

Conflict of Interest

The authors have no conflict of interest.

Authorship Contributions

Participated in research design: Ishida, Ullah, Unadkat

Conducted experiments: Ishida

Performed data analysis: Ishida

Contributed new reagents: Tóth, Juhasz

Contributed to the writing of the manuscript: Ishida, Ullah, Tóth, Juhasz, Unadkat

References

Chenu C and Berteloot A (1993) Allosterism and Na^+-D-glucose cotransport kinetics in rabbit jejunal vesicles: compatibility with mixed positive and negative cooperativities in a homo- dimeric or tetrameric structure and experimental evidence for only one transport protein involved. *J Membr Biol* **132**:95-113.

Endres CJ, Moss AM, Ke B, Govindarajan R, Choi DS, Messing RO and Unadkat JD (2009) The role of the equilibrative nucleoside transporter 1 (ENT1) in transport and metabolism of ribavirin by human and wild-type or Ent1-/- mouse erythrocytes. *J Pharmacol Exp Ther* **329**:387-398.

Fattinger K, Cattori V, Hagenbuch B, Meier PJ and Stieger B (2000) Rifamycin SV and rifampicin exhibit differential inhibition of the hepatic rat organic anion transporting polypeptides, Oatp1 and Oatp2. *Hepatology* **32**:82-86.

He J, Yu Y, Prasad B, Link J, Miyaoka RS, Chen X and Unadkat JD (2014) PET imaging of Oatp-mediated hepatobiliary transport of [(11)C] rosuvastatin in the rat. *Mol Pharm* **11**:2745-2754.

Ho RH, Tirona RG, Leake BF, Glaeser H, Lee W, Lemke CJ, Wang Y and Kim RB (2006) Drug and bile acid transporters in rosuvastatin hepatic uptake: function, expression, and pharmacogenetics. *Gastroenterology* **130**:1793-1806.

Hsiao P and Unadkat JD (2012) P-glycoprotein-based loperamide-cyclosporine drug interaction at the rat blood-brain barrier: prediction from in vitro studies and extrapolation to humans. *Mol Pharm* **9**:629-633.

Hsiao P and Unadkat JD (2014) Predicting the outer boundaries of P-glycoprotein (P-gp)-based drug interactions at the human blood-brain barrier based on rat studies. *Mol Pharm* **11**:436-444.

Ishida K, Ullah M, Tóth B, Juhasz V and Unadkat JD (2018) Successful prediction of in vivo hepatobiliary clearances and hepatic concentrations of rosuvastatin using sandwich-cultured rat hepatocytes, transporter-expressing cell lines, and quantitative proteomics. *Drug Metab Dispos* **46**:66-74.

Ismair M (2003) Interactions of glycyrrhizin with organic anion transporting polypeptides of rat and human liver. *Hepatol Res* **26**:343-347.

Li R, Barton HA and Varma MV (2014) Prediction of pharmacokinetics and drug-drug interactions when hepatic transporters are involved. *Clin Pharmacokinet* **53**:659-678.

Malo C and Berteloot A (1991) Analysis of kinetic data in transport studies: new insights from kinetic studies of Na^+-D-glucose cotransport in human intestinal brush-border membrane vesicles using a fast sampling, rapid filtration apparatus. *J Membr Biol* **122**:127-141.

Prasad B and Unadkat JD (2015) The concept of fraction of drug transported (ft) with special emphasis on BBB efflux of CNS and antiretroviral drugs. *Clin Pharmacol Ther* **97**:320-323.

Shirasaka Y, Mori T, Murata Y, Nakanishi T and Tamai I (2014) Substrate- and dose-dependent drug interactions with grapefruit juice caused by multiple binding sites on OATP2B1. *Pharm Res* **31**:2035-2043.

Shitara Y, Sugiyama D, Kusuhara H, Kato Y, Abe T, Meier PJ, Itoh T and Sugiyama Y (2002) Comparative inhibitory effects of different compounds on rat oatpl (slc21a1)- and Oatp2 (Slc21a5)-mediated transport. *Pharm Res* **19**:147-153.

Wang L, Prasad B, Salphati L, Chu X, Gupta A, Hop CE, Evers R and Unadkat JD (2015) Interspecies variability in expression of hepatobiliary transporters across human, dog, monkey, and rat as determined by quantitative proteomics. *Drug Metab Dispos* **43**:367-374.

Westholm DE, Salo DR, Viken KJ, Rumbley JN and Anderson GW (2009) The blood-brain barrier thyroxine transporter organic anion-transporting polypeptide 1c1 displays atypical transport kinetics. *Endocrinology* **150**:5153-5162.

Footnotes

a) This work was supported by a Postdoctoral Fellowship to KI from F. Hoffmann-La Roche Ltd.

DMD Fast Forward. Published on June 11, 2018 as DOI: 10.1124/dmd.118.080770
This article has not been copyedited and formatted. The final version may differ from this version.

Legends to Figures

Figure 1. Time Course of RSV or OLM Uptake into Oatp- or Ntcp-expressing Cell Lines

The uptake of drugs into Oatp-expressing cells (A-F) was determined in the presence and absence of 100 μM rifamycin SV (Rif SV). The uptake of RSV (G) or OLM (H) into CHO-Ntcp cell lines was evaluated in the presence and absence of extracellular Na^+. RSV was transported by Oatp1a1 (A), 1a4 (C), and 1b2 (E) but not by Ntcp (G). In contrast, OLM was transported by only Oatp1b2 (F) but not by Oatp1a1 (B), 1a4 (D) or Ntcp (H). Note the different y-axis scale in each panel. The data represent the mean ± S.D. of triplicates.

Figure 2. Estimation of Kinetics of Uptake of RSV (A-C) or OLM (D) by CHO-Oatp1a1, HEK293-Oatp1a4, HEK293-Oatp1b2 or the corresponding mock-transfected Cells

Oatp1a1 transported RSV with higher affinity than Oatp1b2 or Oapt1a4 (Table 1). In addition, Oatp1b2 transported RSV with higher affinity than OLM (Table 1). Uptake was conducted in duplicate at all drug concentrations. The predicted lines were obtained by fitting a single binding site Michaelis-Menten model to the uptake data using Phoenix®.

Figure 3. Effect of Various Inhibitors (10 or 100 μM) on Oatp-mediated Uptake of RSV, E17βG or OLM

Ibuprofen (100 μM) and olmesartan acid (100 μM) appeared to be selective inhibitors of Oatp1b2. On the other hand, digoxin (10 μM) and quinine (10 μM) appeared to be selective inhibitors of Oatp1a4. Rifampin (10 μM) inhibited only Oatp1a4 and 1b2, whereas rifamycin SV (10 μM) inhibited only Oatp1a1 and 1b2. BSP and glyburide inhibited all three rat hepatic Oatps. The data are mean ± S.D. of triplicates. †p<0.05; significantly different from the corresponding control (i.e. without the inhibitor). *p<0.05; significant difference between Oatp1a1 and Oatp1a4.

#$p<0.05$; significant difference between Oatp1a1 and Oatp1b2. ‡$p<0.05$; significant difference between Oatp1a4 and Oatp1b2.

Figure 4. Concentration-dependent Inhibition of RSV or OLM Uptake into Oatp-expressing Cell Lines by Rifampin (A-D), Rifamycin SV (E-H), or Digoxin (I-L)

Rifampin inhibited only Oatp1a4 and 1b2. In contrast, rifamycin SV and digoxin were potent inhibitors of Oatp1b2 and Oatp1a4, respectively. The lines are the model predicted values (Phoenix®).

Figure 5 Proposed Experimental Design to Distinguish Ntcp-, Oatp-, and Passive Diffusion-mediated Uptake of Drugs by rat hepatic Oatps

Table 1 Kinetics of Uptake of RSV or OLM by the Rat Hepatic Oatps

Oatp	Substrate	K_m (μM)	V_{max} (pmol/min/mg protein)	H	K_d (μL/min/mg protein)	CL_{int} (V_{max}/K_m) (μL/min/mg protein)
1a1	RSV	9.61 ± 3.97	3594 ± 1152	0.97 ± 0.02	56.8 ± 19.4	386 ± 53
1a4	RSV	67.2 ± 17.1	3077 ± 67	0.98 ± 0.01	7.56 ± 2.21	47.2 ± 11.5
1b2	RSV	28.1 ± 14.8	2242 ± 970	0.93 ± 0.03	10.1 ± 4.9	86.1 ± 21.5
	OLM	72.8 ± 23.9	2169 ± 485	0.94 ± 0.01	6.18 ± 1.36	30.6 ± 3.6

Each experiment was conducted in duplicate, and parameters were estimated using Phoenix®. The values are mean ± SD of 3 independent experiments. H; Hill coefficient.

Table 2 IC_{50} and Hill Coefficient of Inhibitors of Oatp-mediated Uptake of RSV or OLM

Oatp	Substrate	Parameter	BSP	Rifamycin SV	Quinine	Rifampin	Ibuprofen	Olmesartan	Digoxin
1a1	RSV	IC_{50} (μM)	3.00 ± 0.25	3.33 ± 0.28	72.8 ± 6.5	110 ± 7	485 ± 52	612 ± 43	N.I.
		H	1.12 ± 0.06	1.08 ± 0.09	0.826 ± 0.057	1.63 ± 0.12	1.23 ± 0.19	0.787 ± 0.090	N.D.
1a4	RSV	IC_{50} (μM)	6.24 ± 1.07	20.5 ± 2.9	1.89 ± 0.31	1.31 ± 0.23	N.I.	N.I.	0.107 ± 0.015
		H	0.687 ± 0.087	0.746 ± 0.074	0.572 ± 0.048	0.704 ± 0.074	N.D.	N.D.	0.575 ± 0.048
1b2	RSV	IC_{50} (μM)	0.397 ± 0.040	0.140 ± 0.007	125 ± 19	1.12 ± 0.68	48.5 ± 5.1	23.1 ± 4.0	N.I
		H	0.938 ± 0.078	1.26 ± 0.06	0.836 ± 0.127	0.752 ± 0.032	0.622 ± 0.042	0.930 ± 0.107	N.D.
1b2	OLM	IC_{50} (μM)	0.210 ± 0.050	0.088 ± 0.009	150 ± 30	0.583 ± 0.053	61.4 ± 13.0	N.D.	N.I.
		H	1.28 ± 0.29	1.44 ± 0.18	0.745 ± 0.178	0.835 ± 0.063	0.656 ± 0.119	N.D.	N.D..

These parameters were estimated using the data in Figure 4 and Supplemental Figure 3. The data represent the mean ± SE estimated by Phoenix®.

N.I.: not inhibited by 100 μM digoxin or 1000 μM

N.D.: not determined.

DMD Fast Forward. Published on June 11, 2018 as DOI: 10.1124/dmd.118.080770
This article has not been copyedited and formatted. The final version may differ from this version.

Table 3 Excellent Agreement Between the Observed and Predicted Magnitude of Inhibition by Rifampin of the *In Vivo* RSV Sinusoidal Uptake Clearance in the Rat as Measured by PET Imaging

	Sinusoidal uptake clearance (mL/min/kg body weight)	
	Observed[a]	Predicted[b]
Rifampin (-)	70.95 ± 2.88	80.44 ± 13.05
Rifampin (+)	37.28 ± 1.48	45.69 ± 7.95
% Rifampin (-)	52.5%	56.8%

[a]Observed data are from our previous PET imaging study where the mean unbound concentration of rifampin after administration (40 mg/kg IV bolus plus 1.85 mg/min/kg IV infusion) was 9.4 μM (He et al., 2014).

[b]The *in vivo* predicted sinusoidal uptake clearance in the absence of rifampin was estimated by K_m, V_{max}, and K_d (Table 1) and the abundance of Oatp protein as reported previously (Ishida et al., 2018). The *in vivo* predicted sinusoidal uptake clearance in the presence of rifampin was calculated by Eq. 2, and the % remaining activity of each Oatp in the presence of 9.4 μM rifampin (94.8%, 10.5%, and 18.9% for Oatp1a1, 1a4, and 1b2, respectively) was obtained from Fig. 4A-C.

DMD Fast Forward. Published on June 11, 2018 as DOI: 10.1124/dmd.118.080770
This article has not been copyedited and formatted. The final version may differ from this version.

Figure 1

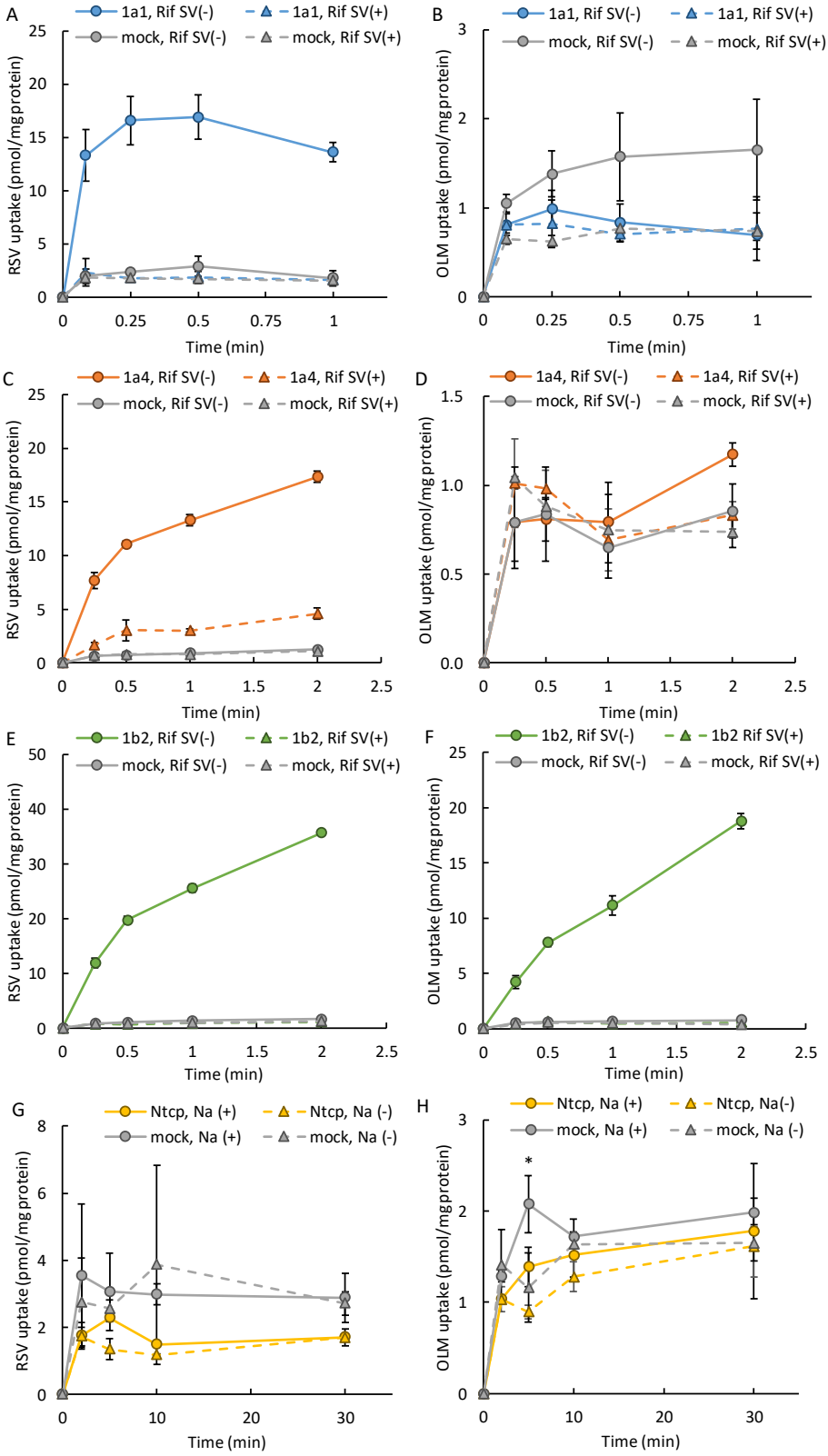

DMD Fast Forward. Published on June 11, 2018 as DOI: 10.1124/dmd.118.080770
This article has not been copyedited and formatted. The final version may differ from this version.

Figure 2

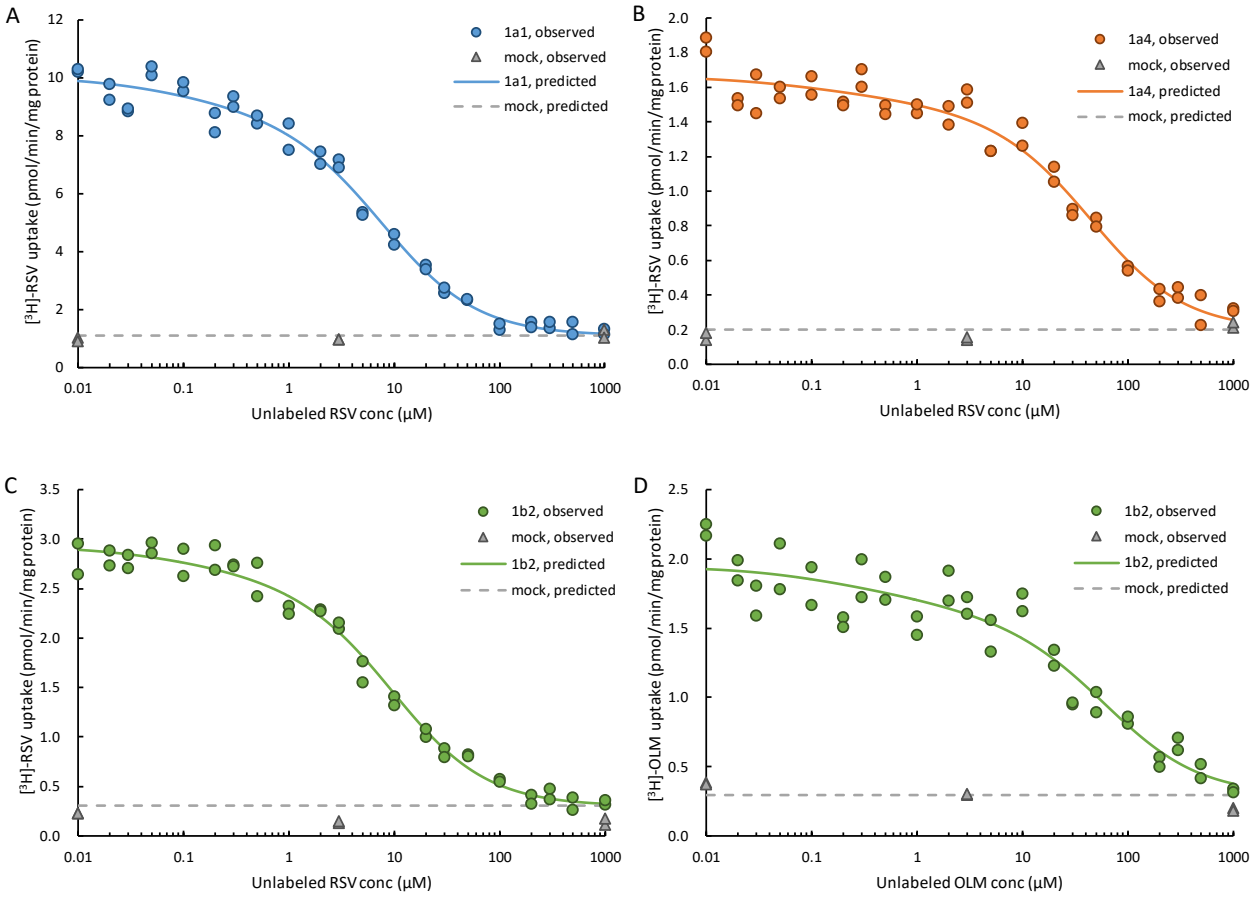

DMD Fast Forward. Published on June 11, 2018 as DOI: 10.1124/dmd.118.080770
This article has not been copyedited and formatted. The final version may differ from this version.

Figure 3

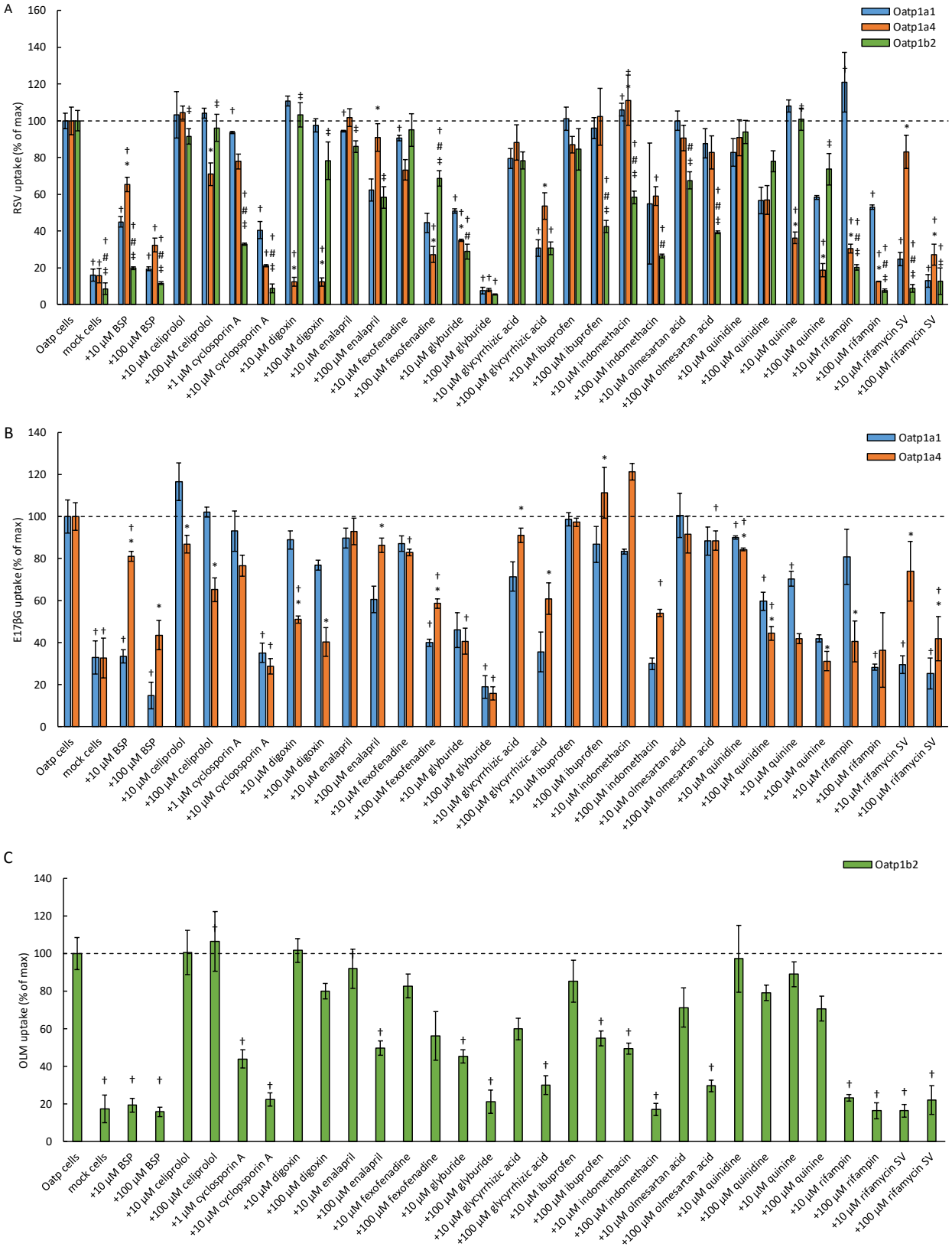

DMD Fast Forward. Published on June 11, 2018 as DOI: 10.1124/dmd.118.080770
This article has not been copyedited and formatted. The final version may differ from this version.

Figure 4

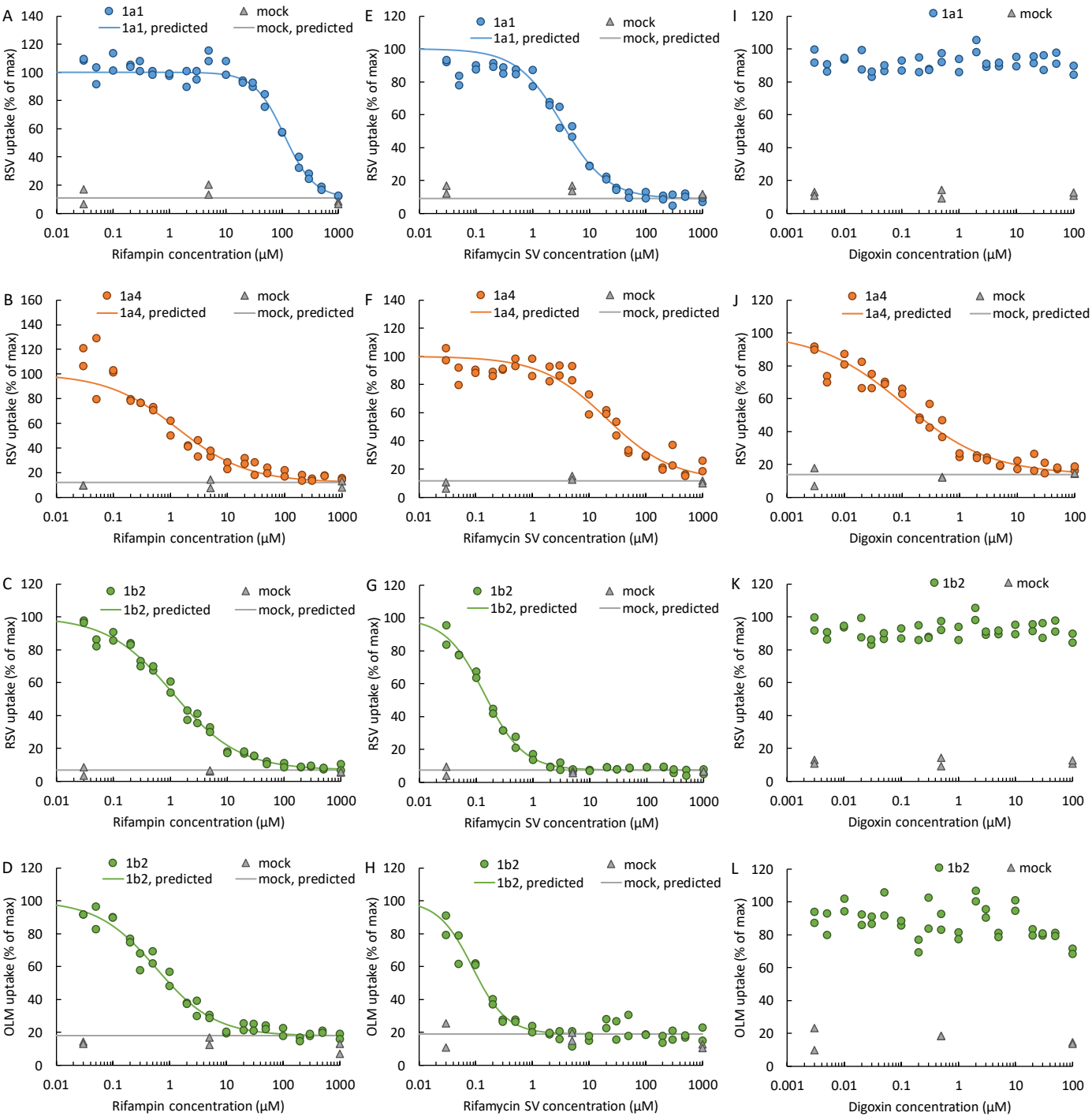

DMD Fast Forward. Published on June 11, 2018 as DOI: 10.1124/dmd.118.080770
This article has not been copyedited and formatted. The final version may differ from this version.

Figure 5